

*Short Communication*

## **Effect of Oxidation Treatment on Microstructure and Electrochemical Properties of 6061 Aluminum Alloy**

*Zhisheng Wang, Yanhua Lei, KunChen, QingHong Li, Yansheng Yin, Runhua Fan*

College of Ocean Science and Engineering, Shanghai Maritime University, 1550 Hai gang Avenue, Shang hai201306, China

\*E-mail: [rhfan@shmtu.edu.cn](mailto:rhfan@shmtu.edu.cn)

*Received: 29 September 2020 / Accepted: 12 November 2020 / Published: 31 December 2020*

---

In this paper, 6061 Al alloy was used as the matrix to prepare the anodic film by acidification. SEM, XRD and EDS were used to study the effect of oxidation treatment on the structure and corrosion resistance of 6061 Al alloy. The results show that the grain size of 6061 Al alloy is larger, and the second phase particles are distributed in the grain. After oxidation treatment, fine second phase particles were precipitated in the grains, resulting in the increase of the strength of 6061 Al alloy. The tensile and impact fracture of 6061 Al alloy treated by oxidation shows the characteristics of intergranular fracture. Surface anodic oxidation treatment can significantly reduce the mechanical property loss of 6061 Al alloy. Compared with bare materials, the initiation and expansion of intercrystalline corrosion can be effectively inhibited, and the strength and plasticity loss of 6061 Al alloy can be reduced, so that 6061 Al alloy anodized with sulfuric acid has better strength.

---

**Keywords:** 6061 Al alloy; Intergranular corrosion; Oxidation treatment; Organizational structure; Mechanical property

### **1. INTRODUCTION**

Because Al alloy has many excellent properties, such as low density, it has been applied to various economic fields and life. However, it is not enough to have the advantages mentioned above, and it is necessary to further improve the thickness of Al oxide film formed on the surface of Al and the characteristics of corrosion resistance [1-3]. Many researchers have extensively studied and improved the surface film properties of Al alloy, making it widely used in various fields of economy [4-6]. Al is the metal material with the largest usage and the most extensive application area among non-ferrous metals, and its application scope is still expanding [7-9]. Al and Al alloys are widely used in transportation, aerospace and other industries because of their excellent properties such as low density, high plasticity, corrosion resistance [10-12]. When the fresh surface of metallic Al is exposed to the atmosphere, it is immediately covered with a very thin oxide film, which will regenerate quickly once

damaged [13]. Anodic oxidation is the most widely applied and successful technology in the surface technology of Al, as well as the most in-depth and comprehensive technology in research and development[7,14-16]. The anodic oxidation film of Al has a series of superior physical and chemical properties, which improves the service life of Al products and is widely used in various fields of life and industry[17-19].

## 2. EXPERIMENTAL

### 2.1. Sample preparation

The main materials used in the experiment: 6061 Al alloy. The components in the supply state of 6061 Al alloy are listed in Table 1. The samples with dimension of  $10 \times 10 \times 3$  mm were cut. The specimens were mechanically ground using SiC papers with grit sizes of 240, 400, 800, 1200 and then degreased in acetone and ethanol, and finally washed in pure water.

After the cleaning and rusting process, the samples were dried for 24 h, and the solution was placed at room temperature and humidity for some time. The corrosive medium employed was a solution of  $\text{Na}_2\text{SO}_4$  (0.5 mol/L). The pH of the medium was adjusted to 2, 3, and 5 by dropwise addition of  $\text{H}_2\text{SO}_4$  to the  $\text{Na}_2\text{SO}_4$  solution at  $22^\circ\text{C}$  (humidity was 50% RH) for 9 days. The applied electrochemical test medium and immersion test medium used the same solution.

**Table 1.** Chemical compositions of 6061 Al alloys (wt.%)

Material	Cu	Mn	Mg	Zn	Cr	Ti	Si	Fe	Zr	Al
wt.%	0.20	0.11	0.99	0.008	0.21	0.015	0.51	0.32	0.05	allowance

### 2.2 Oxidation treatment

In this experiment, the anodizing treatment process with sulfuric acid is as following: 20% sulfuric acid, 20 g/L Al ion, current density =  $2\text{A}/\text{dm}^2$ , concentrated sulfuric acid, oxidation voltage 18 V and 22 V, oxidation temperature  $24^\circ\text{C}$ , and oxidation time 60 min. For study the effect of anodizing treatment, some sample were oxidized under  $350^\circ\text{C}$  for 4 hours. After the 6061 Al alloy samples were processed into plate samples and tensile samples (the size of the plate samples was  $20\text{ mm} \times 20\text{ mm} \times 3\text{ mm}$ ). The bare 6061 Al alloy was labeled as sample 1, and the 6061 Al alloy anodized by sulfuric acid was labeled as sample 2, respectively. After cleaning and drying the flat and tensile samples, there were 5 parallel samples in each group of tensile samples. After grinding and polishing, the microstructure of 6061 Al alloy samples in supply state and oxidation state was observed under JSM-7500F(SEM) scanning electron microscope. The phase composition was analyzed by D/Max-B type rotating anode X-ray(XRD). Tensile test was carried out on CM T5105 microcomputer controlled electronic universal test machine[1]. The  $10\text{ mm} \times 10\text{ mm} \times 3\text{ mm}$  Charpy notch non-standard sample was used for room

temperature impact test on JB300C impact test machine with a pendulum [2]. INCA energy spectrometer was used for element composition analysis of micro regions.

## 2.2 Characterization test

Jsm-7500F scanning electron microscope(SEM) was used to observe the morphology of the surface and cross section, and EDS was used to analyze the composition of the products. D/Max2500V X-ray(XRD) was used to analyze the phase structure before and after the anodic oxidation film treatment. The tube pressure and tube flow were 40 kV and 100 mA respectively. The scanning range was  $20^{\circ} \sim 80^{\circ}$  and the scanning rate was  $10^{\circ}/\text{min}$ . The electrochemical properties of the as-obtained samples were characterized on an electrochemical workstation (Gamry, 1010E), using a three-electrode system (the auxiliary electrode was a platinum wire, the reference ELECTRODE was calomel saturated electrode, and the working electrode was the 6061 Al alloys sample). A copper wire was drawn on the back of the sample, while the rest of the surface was coated with epoxy resin and dried in oven for 24 h. Before testing, the working electrode was cleaned and polished. The excitation signal used for electrochemical impedance spectroscopy (EIS) was 10 mV, while the frequency range was  $10^4 \sim 10^{-2}\text{Hz}$ , which was measured at the self-etching potential using Zview software to analyze the results.

## 3. RESULTS AND DISCUSSION

### 3.1 Corrosion morphology observation

FIG. 1 shows the surface morphology of 6061 Al alloy under different treatments. It can be seen from the figure that the grain of the Al alloy under oxidation treatment is obviously refined. FIG.2 shows the scanning electron microscope and energy spectrum images of 6061 Al alloy treated by oxidation. It can be seen that the second phase of granular short bar is distributed in the grain of the Al alloy, and the energy spectrum shows that its main components are Al, Mg and Si.

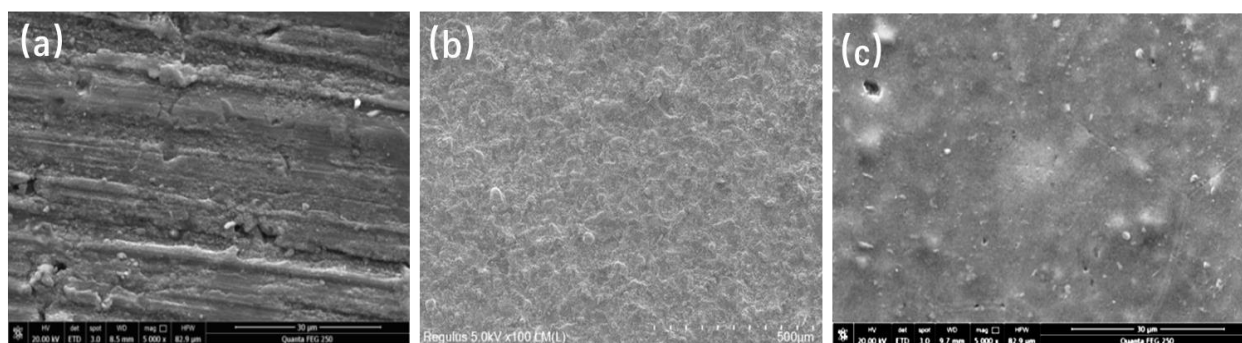


**Figure 1.** Microstructure of sample surface (a: Oxidized under  $350^{\circ}\text{C}$  for 4h, b: Anodizing Oxidation treatment at 22 V, c: Oxidation treatment at 22 V and followed with heat treatment under  $350^{\circ}\text{C}$  for 4 hours)

Due to the oxidation treatment, the original grain of Al alloy is broken to form sub crystal. Subsequently, under the action of oxidation treatment, a large number of crystal nuclei are formed at the place with high grain boundary energy and the coarse second phase particles, so that the grains are refined [20-21].

### 3.2 Effect of oxidation treatment on phase composition of oxide film

Figure 2 shows the XRD pattern after treatment. It can be seen that the oxide film before treatment is mainly composed of  $\gamma$ - $\text{Al}_2\text{O}_3$  phase. After oxidation treatment, the oxidation film was still dominated by  $\gamma$ - $\text{Al}_2\text{O}_3$  phase, but there was a small amount of  $\alpha$ - $\text{Al}_2\text{O}_3$ [22]. As can be seen from Figure 3, the surface morphology of the cross section structure of untreated 6061 Al alloy under the microscope shows that the grain size of 6061 Al alloy is 30~220  $\mu\text{m}$ , and there are a large number of second phase in the structure, and the distribution of the second phase has obvious regularity. TEM image was further used to analyze the precipitated phase inside 6061 Al alloy, and the results were shown in FIG. 2. A large number of precipitated phase Al-Fe-Si existed inside the Al alloy.

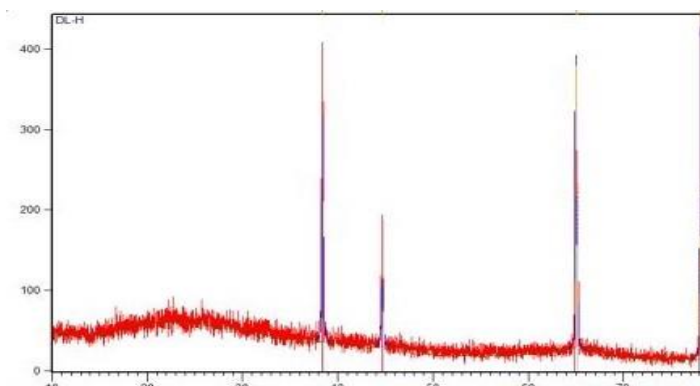


**Figure 2.** XRD patterns of ceramic coatings under anodizing oxidation treatment at 18 V for 1 hour.

### 3.3 Effect of oxidation treatment on the cross section structure of 6061 Al alloy

It can be seen from Figure 3 that the thickness of grain boundary phase is sub-micron level after anodizing oxidization treatment at 18V for 1 h , followed with heating treatment under 350°C for 4 hours. At the same time, a large number of fine second phase compounds are precipitated in the grains. The precipitation of compounds is the most important structural change characteristic of 6061 Al alloy in the oxidation process, and has a significant influence on its performance. On the one hand, the precipitation of the second phase of these compounds results in the decrease of alloying element content, but a large number of nano particles are formed in the grain after the oxidation treatment at 24°C for 1 hour, which is the main reason for the significant improvement of the strength and hardness of 6061 Al alloy[3]. On the other hand, due to the inhibition effect of grain boundary and the second relative dislocation motion and plastic deformation within the grain, the tensile plasticity of 6061 Al alloy after

being oxidized at 24°C for 1 hour significantly decreased. At the same time, the grains were obviously coarsely changed into spherical particles, and the number of grains decreased obviously.

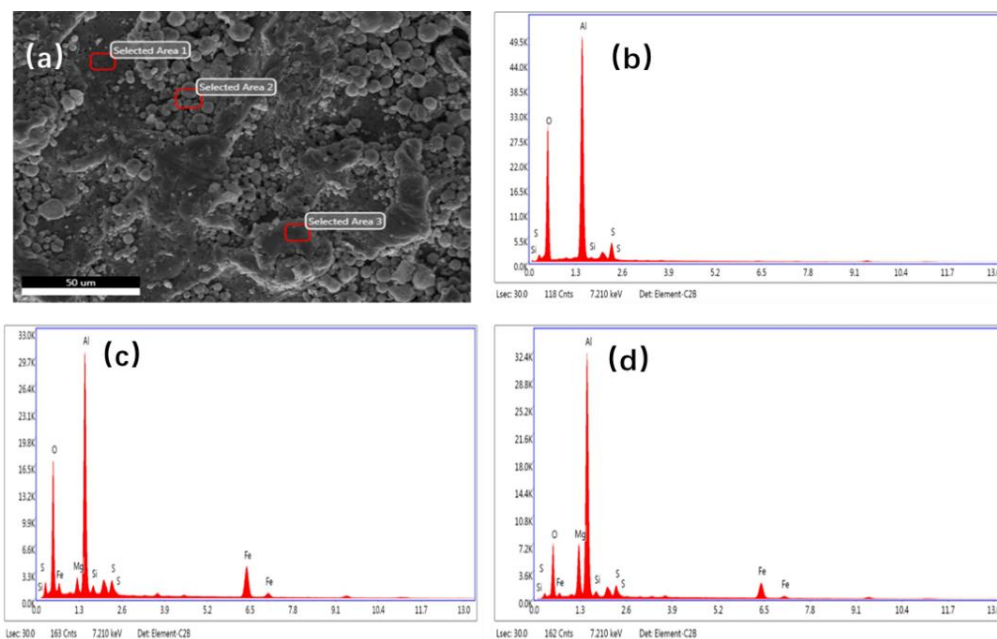


**Figure 3.** Energy spectrum of Al alloy after 1 hour oxidation treatment at 18 V , followed with heat treatment under 350°C for 4 hours.

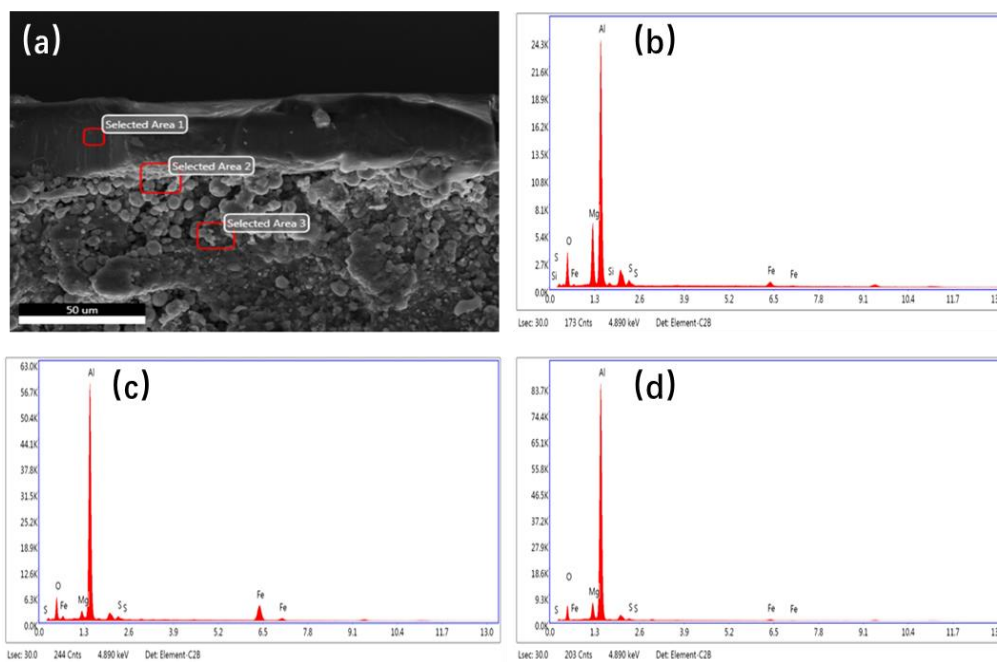
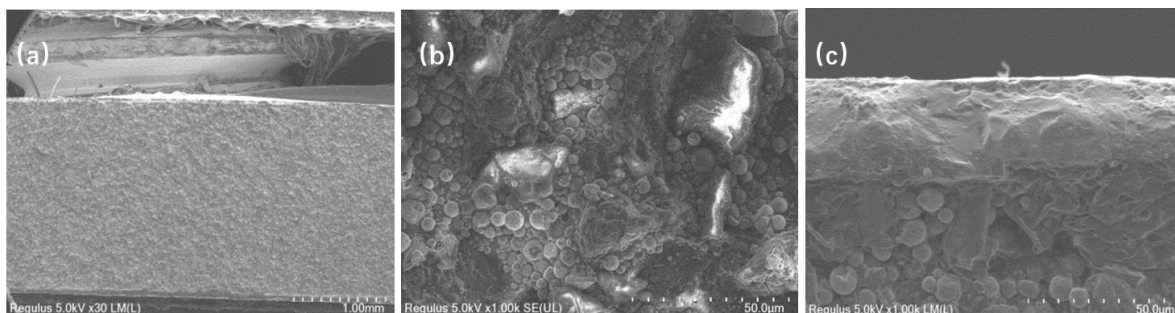


**Figure 4.** SEM images and EDS spectra of the original 6061 Al alloy samples after 4 hours oxidization treatment under 350°C.

FIG. 4 shows the scanning electron microscope and energy spectrum images of the original 6061 Al alloy samples after heat treatment at 350°C for 4 hours. It can be seen that the grain of the Al alloy is distributed with granular or long and short rod-like second phase, and the energy spectrum shows that the main components are Al, O, Mg and Si, that is, the ternary compound Al, Mg and Si is the main strengthening phase of the Al alloy.

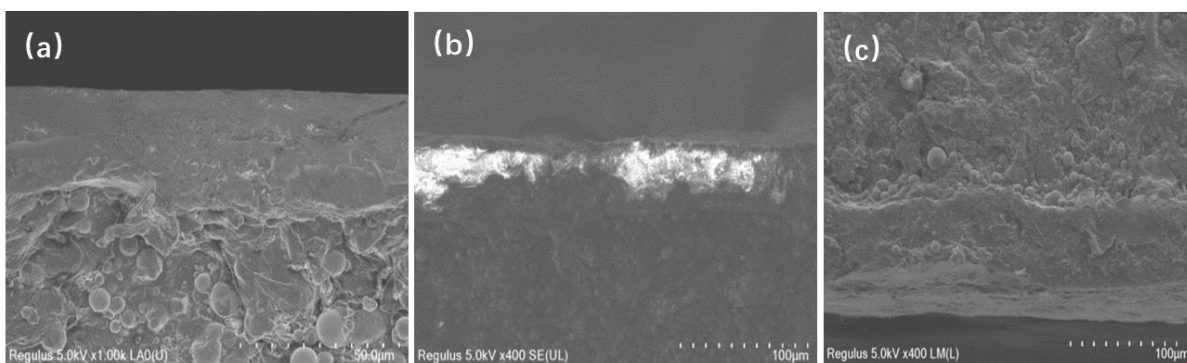
### 3.4 Effect of oxidation treatment on fracture morphology and fracture mechanism of 6061 Al alloy

Figure 5 displays the SEM morphology of the tensile fracture of the 6061 Al alloy treated at different conditions. As shown in Figure 5a, the original tensile fracture characteristics of 6061 Al alloy is obviously, with uniform grain size distribution. However, the tensile fracture for the sample after 1 hour anodization treatment at 18 V, as in Fig. 5b were the intergranular brittle fracture characteristics, this is because the oxidation process of 6061 Al alloy after a large amount of precipitation, grain boundary at the same time, because of low bonding strength of 6061 Al alloy grain boundary after oxidation treatment led to the fracture. Compared with the supply of 6061 Al alloy after oxidation treatment, the tensile fracture surface of 6061 Al alloy after anodizing oxidation treatment at 18 V for 1 hour is smoother and has worse plasticity.



**Figure 5.** SEM morphology of tensile fracture of 6061 Al alloy ( a: Oxidized under 350°C for 4h, b: Anodizing Oxidation treatment at 22 V, c: Anodizing oxidation treatment at 22 V and followed with heat treatment under 350°C for 4 hours)

SEM morphology of impact fracture of the 6061 Al alloy is shown in Figure 6. There are dimples of different sizes on the impact section of untreated 6061 Al alloy, and a large number of spherical inclusion particles are distributed, as shown in FIG. 6a, where crack initiation is easy. The main body of impact fracture of 6061 Al alloy after oxidation treatment shows the characteristics of intergranular brittle fracture. As shown in FIG. 6b, the dispersion of the second phase particles in 6061 Al alloy after anodic oxidation at 18 V for 1 hour has a strong inhibiting effect on crack growth. Therefore, the Al alloy after anodic oxidation at 18 V for 1 hour has a higher impact toughness instead. According to the literature [9], the impact toughness of 6061 Al alloy decreases significantly after aging at 350°C for 4 h.



**Figure 6.** Impact fracture SEM morphology of 6061 AlAl alloy (a:Unoxidized treatment, b:Oxidation treatment, c: Oxidation treatment and 350°C, 4h heat treatment)

### 3.4 Electrochemical measurements

From the literature[8], when the thickness of product increased to a certain level, it formed a protective layer on the matrix, playing a leading role in slowing down the corrosion rate. Figure 6 shows the Nyquist plots of the anodizing treated 6061 Al alloy.

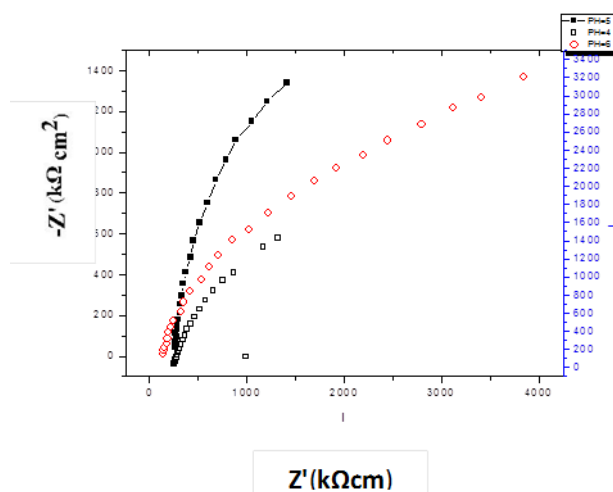


**Figure 7.** Nyquist plots of the anodizing treated 6061 Al alloy 6061 Al alloy at pH=2, 3, and 5

**Table 2.** Impedance parameters of 6061 Al alloy at pH=2, 3, and 5

pH	$R_s(Qcm^{-2})$	$Q(cm^2s^{-n}Q)$	N	$R_t(Qcm^{-2})$
2	4.1	$2.88 \times 10^{-5}$	0.89	$3.67 \times 10^4$
3	5.2	$2.93 \times 10^{-5}$	0.76	$4.55 \times 10^4$
5	5.8	$3.51 \times 10^{-5}$	0.73	$8.94 \times 10^4$

The electrochemical impedance of 6061 Al alloy at pH=2 indicates lower corrosion resistance than at higher pH values. At pH=3, the diameter of capacitive semicircles on day 15 increased significantly

as compared to pH=5. Furthermore, a semi-finite Warburg element (W) appeared on day 15 at pH=2, which illustrates that the electron transfer was mainly controlled by diffusion. The constants of 6061 Al alloy at three different pH values are shown in Figure 6, and the electrochemical parameters are listed in Table 2. The solution impedance ( $R_s$ ) presented different values under the effect of pH=2, 3, and 5, exhibiting highest value of  $R$  in comparison with solutions with lower pH values. Risa criterion presents resistance of electron transfer between the film and matrix metal [9].

As shown in Figure 8, the circuit of metal in the solutions with pH=2,3,5 was found to be  $R_s(QR)(QR)$ . As the pH increased, the corrosion reaction continued and the layer of rust on 6061 Al alloy increased[20-22], leading to a dense film on the surface of 6061 Al alloy. The accumulation of products layer on the surface of the sample directly affects the  $R_p$  value of the sample [21]. The  $R_f$  value following 15 days of exposure to pH=5 was higher in comparison with pH=2 and 3, implying the formation of the protective film on the surface of the sample. According to the EDS analyses of 6061 Al alloy in Figure 2,3 the appearance of Al、Fe、Mg and O confirm that a dense protective film was formed on the 6061 Al alloy surface.

$R_s$  – Solution resistance

$R_p$  – Resistance of electrochemical film

$R_{ct}$  – Charge transfer resistance

$Q_p$  – Resistance of passivated film

$Q_{dl}$  – Double layer capacitance

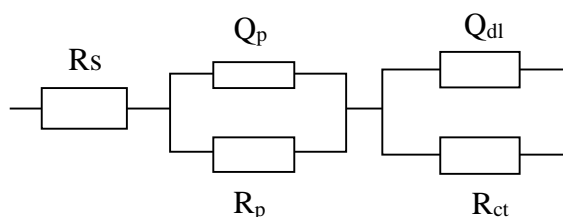


**Figure 8.** Schematic diagram and equivalent electrical circuits used for fitting of EIS diagrams Grams.

#### 4. CONCLUSIONS

Fine second phase particles are distributed within the crystal boundary of the original 6061 Al alloy. After being oxidized at 24°C for 1 hour, the ratio of 6061 Al alloy and the original 6061 Al alloy is obviously refined after being oxidized at 350°C for 4 hours. After anodizing oxidation treatment at 18 V for 1 hour, the grains also precipitated fine particles. The fundamental reason for the plasticity of 6061 Al alloy is the obvious change of its structure during the oxidation treatment. The original impact fracture of 6061 Al alloy and the oxidation treatment of 6061 Al alloy show the characteristics of brittle fracture along the crystal. Therefore, the sulfuric acid anodic oxidation film has a significant protective effect on the matrix and can inhibit the initiation and expansion of intercrystallite corrosion.

#### References

1. X.F. Sheng, Y. Yang, Y.J. Cheng, J. Li, W. Wu, Y. Liu, K. Li, Y.F. Zhao, G.A. He, *J. Alloys compd.*, 845 (2020) 156198
2. B. Seidel, A. Rabenstein, M. Redetzky, A. Wagner, E. Brinksmeier, *Prod.Eng.*, 11(2017)41.
3. S.Z. Kode, A. Bien, M. Antoszkiewicz, *Ceram Int.*, 42(2016)11275.

4. Z. Zheng, Y.L. Deng, W.B. Zhu, F.Q. Wang, K.D. Jiang, X.B. Guo, *J. Alloys Compd.*, 846 (2020) 156233.
5. F.S. Pan, M.B. Yang, X.H. Chen, *J. Mater. Sci & Technol.*, 32(2017) 1211-1221. .
6. S. Mokhtari, Fkarimzadeh, M. Habbasi, Raeissik, *Surf. Coat. Tech.*, 324(2017)99.
7. V. P.Singh, S.K. Patel, A. Ranjan, B. Kuriachen, *J. Mater. Res. Technol.*, 9 (2020) 6217-6256.
8. M. Almasi Kashi, A.Ramazani, M. Raoufi, *Thin Solid Films*, 518(2010)6767.
9. A. Balbo, A. Frignani, V. Grassi, F. Zucchi, *Corros. Sci.*, 73(2013)80.
10. T.B. He, S. Chen, T. Lu, *J. Alloys Compd.*, 848(2020)156655.
11. M. Zeidabadinejad. M. Shahidi-Zandi. M. M. Foroughi, H. Asadollahzadeh, *Mater. Corros.*, 70 (2019)1999.
12. Smokhtari, Fkarimzadeh, M. Habbasi, Kraeissi, *Surf. Coat. Tech.*, 324(2017)99.
13. K. Shimizu, K. Kobayashi, G.E. Thompson, *Philos. Mag.*, 66(1992)643.
14. M. Braic, A. Vladescu, V. Braic, C.M. Crotrut and D. Stanciu, *Mater. Corros.*, 66(2015)1331.
15. S.H. Tuna, N.Ö. Pekmez and I. Kürkçüoğlu, *J. Prosthet. Dent.*, 114(2015)725.
16. Y. Ma, X. Zhou, Y. Liao, Y. Yi, H. Wu, Z. Wang, *Corros. Sci.*, 107(2016)41.
17. J S Zhang. *Oxid. Met.*, 80(2013)669
18. Q. Zhang, Y. He, W. Wang, N. Lin, C. Wu, N. Li, *Corros. Sci.*, 94(2015)48.
19. A.N. Beltiukov, E.V. Stashkova, O.V. Boytsova. *Appl. Sur. Sci.*, 459 (2018)583-587.
20. X. Feng, X. Lu, Y. Zuo, N. Zhuang, D. Chen, *Corros. Sci.*, 103(2016)223.
21. M. Chen, H. B. Liu, L. B. Wang, C. X. Wang and V. Ji, *Surf. Coat. Tech.*, 344(2018)132.
22. Y.Xiong, C. Wang, *App. Surf. Sci.*, 322(2014)230.

© 2021 The Authors. Published by ESG ([www.electrochemsci.org](http://www.electrochemsci.org)). This article is an open access article distributed under the terms and conditions of the Creative Commons Attribution license (<http://creativecommons.org/licenses/by/4.0/>).